Phase Equilibria of the Ag–Cu–M (M = Nb, Fe, Pb) Systems

Yu Zhang[1,4] · Biao Hu[1,4] · Huiqing Yin[2] · Shuhong Liu[3] · Yong Du[3]

Abstract Sixteen alloys were prepared to determine the isothermal sections of the Ag–Cu–Nb system at 500, 600 and 700 °C using x-ray diffraction (XRD) and scanning electron microscopy with energy dispersive x-ray spectroscopy (SEM/EDS). Based on the thermodynamic descriptions of constitutive binary systems as well as the experimental phase equilibria data obtained from the present work and literatures, the Ag–Cu–M (M = Nb, Fe, Pb) ternary systems were thermodynamically evaluated by the CALPHAD (CALculation of PHAse Diagrams) method. The solution phases were described by the substitutional solution model and a set of self-consistent thermodynamic parameters was finally obtained for each of the ternary systems. The calculated isothermal sections are in good agreement with most of the reliable experimental data.

Keywords CALPHAD · experimental investigation · phase equilibria · thermodynamic modeling

✉ Biao Hu
hubiao05047071@163.com; bhu@aust.edu.cn

1 School of Materials Science and Engineering, Anhui University of Science and Technology, Huainan 232001, Anhui, People's Republic of China

2 Shanghai Institute of Applied Physics, Chinese Academy of Sciences, Shanghai 201800, People's Republic of China

3 State Key Laboratory of Powder Metallurgy, Central South University, Changsha 410083, Hunan, People's Republic of China

4 Anhui International Joint Research Center for Nano Carbon-Based Materials and Environmental Health, Huainan 232001, Anhui, People's Republic of China

1 Introduction

Ag–Cu based alloys are well known for their good electronic conductivity, higher strength of brazing joints and excellent process performance,[1–3] and have been applied in various industries, such as electronic industry, brazing fillers, and lead frames. As high strength and high conductivity materials, the addition of alloying elements to Ag–Cu alloys can lead to a significant improvement of electrical and mechanical properties through precipitation hardening and solid solution strengthening mechanisms. The Ag–Cu–M (M = Nb, Fe, Pb) systems represent the base of multicomponent Ag–Cu based alloys with Nb and Fe as additional alloying elements in our efforts.[4–6] The addition of Nb and Fe in Ag–Cu alloys improves the wettability of solder and the grain boundary structure of brazing joints through solid solution strengthening. Although Pb-containing solders have been almost completely replaced by lead-free solders in the electronic industry due to its toxicity, for seeking out alternative elements, i.e., Fe, Ni, and Zn, to avoid toxicity and improve oxidation behavior investigation of the phase equilibria of the Ag–Cu–Pb system is still needed. Consequently, the information on the phase equilibria and thermodynamic properties of the Ag–Cu based ternary systems are required for the solders or brazing materials fabrication processing.

There are numerous phase equilibria and thermodynamic studies regarding the constitutive binary and ternary systems except the Ag–Nb system. The phase equilibria of the Ag–Nb system were determined by Kieffer et al.[7] by means of x-ray diffraction (XRD), electrical conductivity and metallographic and the results show that the solubility of Nb in liquid Ag is extremely small. Baren[8] reviewed the data for the Ag–Nb system and reported three solution

Table 1 Nominal compositions, identified phase and compositions of the Ag–Cu–Nb alloys annealed at 500, 600 and 700 °C determined by XRD and SEM/EDS

| Alloy No	Nominal composition, at.%	Annealed time (days)	Annealed temperature, °C	Phases identified	Composition, at.%		
					Ag	Cu	Nb
A1	$Ag_{70}Cu_{20}Nb_{10}$	60	500	fcc(Ag)	90.03	9.12	0.85
				fcc(Cu)	4.46	89.13	6.41
				bcc(Nb)	…	…	…
A2	$Ag_{10}Cu_{50}Nb_{40}$	60	500	fcc(Ag)	87.78	11.85	0.37
				fcc(Cu)	2.68	93.27	4.05
				bcc(Nb)	0.76	1.44	97.80
A3	$Ag_{30}Cu_{60}Nb_{10}$	60	500	fcc(Ag)	90.44	8.94	0.62
				fcc(Cu)	4.58	88.77	6.65
				bcc(Nb)	1.15	2.13	96.72
A4	$Ag_{15}Cu_{65}Nb_{20}$	60	500	fcc(Ag)	94.33	4.63	1.04
				fcc(Cu)	4.32	89.40	6.28
				bcc(Nb)	…	…	…
B1	$Ag_{70}Cu_{20}Nb_{10}$	50	600	fcc(Ag)	91.56	7.99	0.45
				fcc(Cu)	2.21	97.59	0.20
				bcc(Nb)	…	…	…
B2	$Ag_{35}Cu_{30}Nb_{35}$	50	600	fcc(Ag)	90.03	9.46	0.51
				fcc(Cu)	2.13	97.43	0.44
				bcc(Nb)	0.22	0.99	98.79
B3	$Ag_{30}Cu_{60}Nb_{10}$	50	600	fcc(Ag)	89.42	10.18	0.40
				fcc(Cu)	1.97	97.83	0.20
				bcc(Nb)	0.50	2.39	97.11
B4	$Ag_{10}Cu_{50}Nb_{40}$	50	600	fcc(Ag)	90.50	9.19	0.31
				fcc(Cu)	1.91	97.77	0.32
				bcc(Nb)	0.49	5.48	94.03
C1	$Ag_{70}Cu_{20}Nb_{10}$	40	700	fcc(Ag)	88.46	11.28	0.26
				fcc(Cu)	3.53	96.07	0.40
				bcc(Nb)	0.51	5.21	94.28
C2	$Ag_{40}Cu_{30}Nb_{30}$	40	700	fcc(Ag)	88.72	10.83	0.45
				fcc(Cu)	3.47	96.26	0.27
				bcc(Nb)	…	…	…
C3	$Ag_{25}Cu_{25}Nb_{50}$	40	700	fcc(Ag)	88.55	10.37	1.08
				fcc(Cu)	2.31	97.29	0.40
				bcc(Nb)	…	…	…
C4	$Ag_{47}Cu_{45}Nb_{8}$	40	700	fcc(Ag)	88.17	11.44	0.39
				fcc(Cu)	2.62	96.66	0.72
				bcc(Nb)	0.34	6.07	93.59

phases, liquid, fcc(Ag) and bcc(Nb), and an invariant reaction, liquid + bcc(Nb) → fcc(Ag).

So far, no phase equilibria data and thermodynamic properties of the Ag–Cu–Nb ternary system have been reported in the literature and the present work was dedicated to determining the isothermal sections of the Ag–Cu–Nb system at 500, 600 and 700 °C. The phase equilibria of the Ag–Cu–Fe system at 1207 and 1550 °C were

J. Phase Equilib. Diffus. (2022) 43:533–546

535

Fig. 1 The BSE micrographs of the Ag–Cu–Nb alloys at 500, 600 and 700 °C annealed 60, 50 and 40 days, respectively:
(a) alloy A2 ($Ag_{10}Cu_{50}Nb_{40}$);
(b) alloy A4 ($Ag_{15}Cu_{65}Nb_{20}$);
(c) alloy B3 ($Ag_{30}Cu_{60}Nb_{10}$);
(d) alloy B4 ($Ag_{10}Cu_{50}Nb_{40}$);
(e) alloy C1 ($Ag_{70}Cu_{20}Nb_{10}$)
and (f) alloy C4 ($Ag_{47}Cu_{45}Nb_8$)
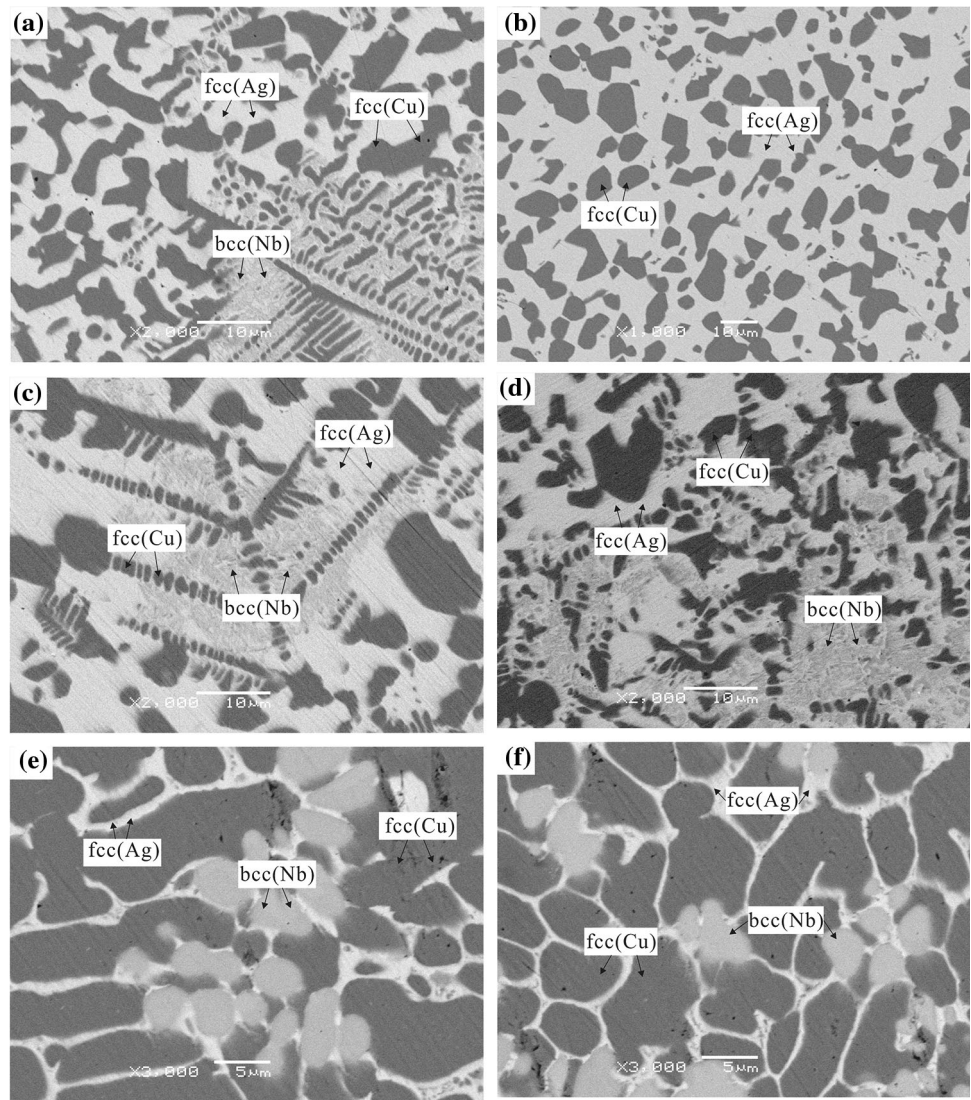
investigated by Aria et al.[9] and Petzow and Effenberg,[10] respectively, and the liquidus projection was investigated by Lüder.[11] The phase boundaries of the liquid /liquid + (αFe) and liquid/liquid#1 + liquid#2 were determined, and no ternary compound was found. Klassen et al.[12] investigated the phase evolution of alloys Ag_{25}-$Cu_{50}Fe_{25}$ and $Ag_{40}Cu_{20}Fe_{40}$ with milling time by XRD and differential scanning calorimetry, and two models based on kinetic and energetic considerations were discussed and compared to the results. It was found that the immiscibility

of Ag and Fe is caused by their high enthalpy of mixing rather than the differences in the mechanical properties or incoherency. Later, microstructure and properties of three Cu–Fe–Ag in situ composites (Cu–12Fe–1Ag, Cu–14Fe–3Ag and Cu–11Fe–6Ag, wt.%) were studied and the distribution of Fe and Ag in the matrix were analyzed by Gao et al.[13] using energy dispersive x-ray spectroscopy. The presence of Ag reduced the solubility of Fe in the matrix at high temperature, and the strength and conductivity of Cu–Fe–Ag composites increased at the same time. Wang
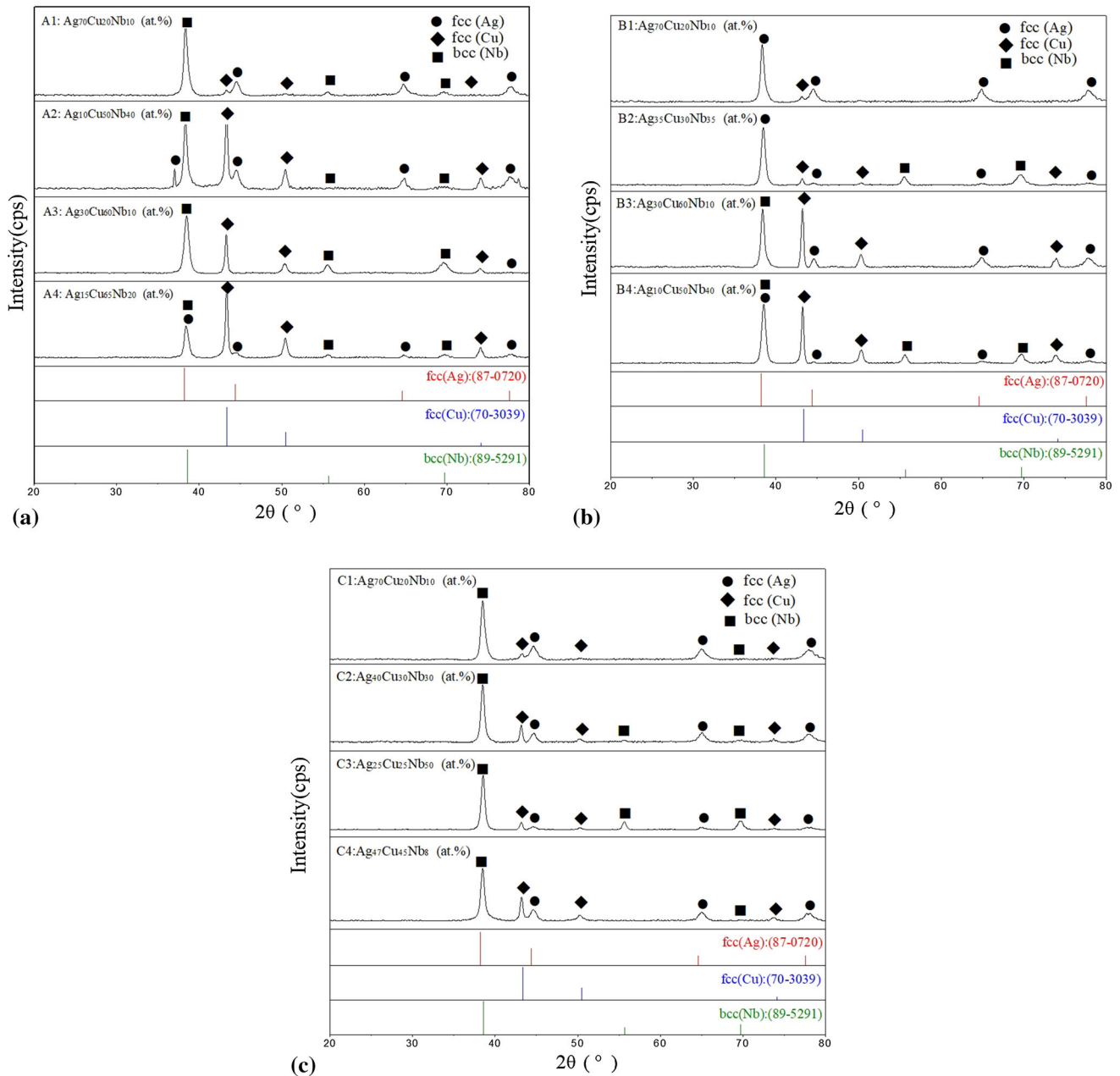
536

J. Phase Equilib. Diffus. (2022) 43:533–546

Fig. 2 XRD patterns of the Ag–Cu–Nb alloys at 500, 600 and 700 °C annealed 60, 50 and 40 days, respectively: (a) alloys A1–A4; (b) alloys B1–B4 and (c) alloys C1–C4

et al.[14] investigated the effect of Ag addition on the diffusion mechanisms of aging precipitation processed Cu–Fe alloys by first-principles calculations. The calculated results agree well with the available experimental observation. The thermodynamic data from literature[10–14] enable finding other suitable alloying elements for preparation of high strength and high conductivity Ag–Cu alloys or in situ composites. For the Ag–Cu–Pb system, the
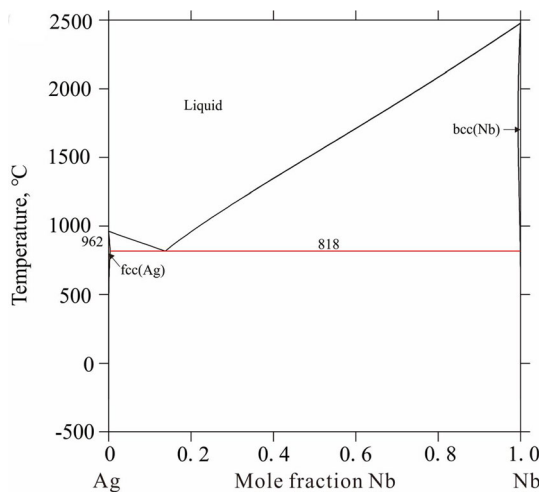
J. Phase Equilib. Diffus. (2022) 43:533–546

537

Fig. 3 The calculated phase diagram of the Ag–Nb system using the thermodynamic parameter from the present work

experimental phase equilibria data at 527 and 727 °C and complete liquidus projection were available from Petzow and Effenberg.[10] One three-phase region Liquid + fcc(Ag) + fcc(Cu) and three two-phase regions, *i.e.*, Liquid + fcc(Ag), Liquid + fcc(Cu) and fcc(Ag) + fcc(Cu), were determined. In the work of Jiang et al.,[15] vapor–liquid equilibria of the Ag–Cu–Pb system were experimentally investigated by vacuum distillation.

The purpose of the present work was to determine microstructure and phase equilibria at 500, 600 and 700 °C in the Ag–Cu–Nb system using XRD and scanning electron microscopy with energy dispersive x-ray spectroscopy (SEM/EDS), and to obtain a set of thermodynamic parameters for the Ag–Cu–M (M = Nb, Fe, Pb) systems using the CALPHAD approach.[16,17]

2 Experimental Procedures

Silver (99.99 wt.%), copper (99.99 wt.%) and niobium (99.99 wt.%) (New Metal Materials Technology Co., Ltd., China) were used as starting materials to determine the phase equilibria of the Ag–Cu–Nb system. Sixteen ternary alloys were designed, and their nominal compositions are listed in Table 1. The alloys were weighed using a high-

precious balance with a sensitivity of 0.0001 g. The designed sixteen ternary alloys with various compositions were melted in a non-consumable vacuum arc-melting furnace (WK-I, Physcience Opto-electronics Co., Ltd. Beijing, China) with water-cooled copper crucible under 99.999% pure Ar (Shanghai Pressure Reducer Factory Co., Ltd.) atmosphere. The experimental pressure of the protective gas is 0.98 MPa. In order to reduce oxygen pollution of the sample during the melting process pure zirconium was first melted to reduce the oxygen amount in the melting vessel. Each alloy was re-melted at least five times to ensure the specimen homogeneous. After arc melting, the mass losses of each sample were less than 1 wt.%. The equilibrated alloys were then wrapped with molybdenum wire, sealed in evacuated quartz capsules with vacuum sealing machine (MRVS-1002, Wuhan Bailibo Technology Co., Ltd., China), and annealed at 500 °C (60 days), 600 °C (50 days) and 700 °C (40 days) in the high temperature diffusion furnace (KSL-1200X, Hefei Kejing Material Technology Co., Ltd., China), followed by quenching in cold water to retain the equilibrium microstructures at high temperature.

The microstructure and phase compositions were obtained from SEM/EDS (JSM-6360LV/GENE-SIS2000XM60, JEOL, Japan) using 20 kV acceleration voltage, 10 μs scanning speed and 4.5 mm working distance. Generally, three points of each phase were measured by EDS analysis and their average value was taken as the phase composition. The powder XRD measurements of the annealed alloys were performed using a Cu-Kα radiation at 40 kV and 300 mA to identify phases. Diffraction patterns were generally acquired with a scan step 0.02° of over a 2θ range 20–80°. The identified phases and compositions of the annealed alloys were listed in Table 1. The phase composition was not calibrated with a standard sample and the error range of the average value compared to the composition of each point is about 1 at.%.

3 Thermodynamic Model

The Gibbs energy functions of the pure elements Ag, Cu, Nb, Fe and Pb were taken from the SGTE database compiled by Dinsdale.[18] The thermodynamic parameters of the Ag–Cu,[19] Ag–Fe,[20] Ag–Pb,[21] Cu–Nb,[22] Cu–Fe[23]

Table 2 Summary of the thermodynamic parameters in the Ag–Cu–M (M = Nb, Fe, Pb) systems

System	Phases/Models	Thermodynamic parameters	References
Ag–Cu–Nb	liquid: (Ag, Cu, Nb)$_1$	$^{0}L_{Ag,Cu}^{liquid} = 16914.949 - 14.7721 \cdot T + 1.54955 \cdot T \cdot \ln(T)$	[19]
		$^{1}L_{Ag,Cu}^{liquid} = -1963.3 + 0.8623 \cdot T$	[19]
		$^{0}L_{Cu,Nb}^{liquid} = 204361.19 - 89.93141 \cdot T$	[22]
		$^{1}L_{Cu,Nb}^{liquid} = -105148.17 + 57.81653$	[22]
	fcc: (Ag, Cu, Nb)$_1$Va$_1$	$^{0}L_{Ag,Cu:Va}^{fcc} = 32580.365 - 7.4547 \cdot T$	[19]
		$^{1}L_{Ag,Cu:Va}^{fcc} = -10144.596 + 5.5617 \cdot T$	[19]
		$^{0}L_{Cu,Nb:Va}^{fcc} = 45699.84 - 5.22785 \cdot T$	[22]
		$^{0}L_{Ag,Nb:Va}^{fcc} = 35002$	This work
		$^{0}L_{Ag,Cu,Nb:Va}^{fcc} = 102011$	This work
	bcc: (Ag, Cu, Nb, Va)$_1$ Va$_3$	$^{0}L_{Ag,Cu:Va}^{bcc} = 12000$	[19]
		$^{0}L_{Cu,Nb:Va}^{bcc} = 49480.18$	[22]
		$^{0}L_{Ag,Nb:Va}^{bcc} = 62000$	This work
	hcp: (Ag, Cu, Nb)$_1$Va$_{0.5}$	$^{0}L_{Ag,Cu:Va}^{hcp} = 25000$	[19]
		$^{0}L_{Cu,Nb:Va}^{hcp} = 20000$	[22]
		$^{0}L_{Ag,Nb:Va}^{hcp} = 15021$	This work
Ag–Cu–Fe	liquid: (Ag, Cu, Nb)$_1$	$^{0}L_{Ag,Cu}^{liquid} = 16914.949 - 14.7721 \cdot T + 1.54955 \cdot T \cdot \ln(T)$	[19]
		$^{1}L_{Ag,Cu}^{liquid} = -1963.3 + 0.8623 \cdot T$	[19]
		$^{0}L_{Ag,Fe}^{liquid} = 81157.09$	[20]
		$^{1}L_{Ag,Fe}^{liquid} = -8743.92$	[20]
		$^{0}L_{Cu,Fe}^{liquid} = 36088 - 2.33 \cdot T$	[23]
		$^{1}L_{Cu,Fe}^{liquid} = 324.53 - 0.03 \cdot T$	[23]
		$^{2}L_{Cu,Fe}^{liquid} = 10355.4 - 3.6 \cdot T$	[23]
		$^{0}L_{Ag,Cu,Fe}^{liquid} = -25977.12$	This work
	fcc: (Ag, Cu, Fe)$_1$Va$_1$	$^{0}L_{Ag,Cu:Va}^{fcc} = 32580.365 - 7.4547 \cdot T$	[19]
		$^{1}L_{Ag,Cu:Va}^{fcc} = -10144.596 + 5.5617 \cdot T$	[19]
		$^{0}L_{Ag,Fe:Va}^{fcc} = 113281.713$	[20]
		$^{0}L_{Cu,Fe:Va}^{fcc} = 48232.5 - 8.61 \cdot T$	[23]
		$^{1}L_{Cu,Fe:Va}^{fcc} = 8861.88 - 5.29 \cdot T$	[23]
	bcc: (Ag, Cu, Fe, Va)$_1$ Va$_3$	$^{0}L_{Ag,Cu:Va}^{bcc} = 12000$	[19]
		$^{0}L_{Ag,Fe:Va}^{bcc} = 124459.792$	[20]
		$^{0}L_{Cu,Fe:Va}^{bcc} = 39258 - 4.14983 \cdot T$	[23]
	hcp: (Ag, Cu, Fe)$_1$Va$_{0.5}$	$^{0}L_{Ag,Cu:Va}^{hcp} = 25000$	[19]
		$^{0}L_{Ag,Fe:Va}^{hcp} = 100000$	[20]
		$^{0}L_{Cu,Fe:Va}^{hcp} = 48232.5 - 8.60954 \cdot T$	[23]
		$^{1}L_{Cu,Fe:Va}^{hcp} = 8861.88 - 5.28975 \cdot T$	[23]

J. Phase Equilib. Diffus. (2022) 43:533–546

539

Table 2 continued

System	Phases/Models	Thermodynamic parameters	References
Ag–Cu–Pb	liquid: $(Ag, Cu, Pb)_1$	$^0L_{Ag,Cu}^{liquid} = 16914.949 - 14.7721 \cdot T + 1.54955 \cdot T \cdot \ln(T)$	[19]
		$^1L_{Ag,Cu}^{liquid} = -1963.3 + 0.8623 \cdot T$	[19]
		$^0L_{Ag,Pb}^{liquid} = 13330.32 - 6.21270 \cdot T$	[21]
		$^1L_{Ag,Pb}^{liquid} = -1449.03 - 1.05718 \cdot T$	[21]
		$^2L_{Ag,Pb}^{liquid} = -2089.13$	[21]
		$^0L_{Cu,Pb}^{liquid} = 31008 - 7.195 \cdot T$	[24]
		$^1L_{Cu,Pb}^{liquid} = 15345 - 10.826 \cdot T$	[24]
		$^2L_{Cu,Pb}^{liquid} = -64931008 + 5.947 \cdot T$	[24]
		$^3L_{Cu,Pb}^{liquid} = -18416 + 13.16 \cdot T$	[24]
		$^0L_{Ag,Cu,Pb}^{liquid} = -23524$	This work
	fcc: $(Ag, Cu, Pb)_1 Va_1$	$^0L_{Ag,Cu:Va}^{fcc} = 32580.365 - 7.4547 \cdot T$	[19]
		$^1L_{Ag,Cu:Va}^{fcc} = -10144.596 + 5.5617 \cdot T$	[19]
		$^0L_{Ag,Pb:Va}^{fcc} = 30325.21 - 5.74345 \cdot T$	[21]
		$^1L_{Ag,Pb:Va}^{fcc} = -3290.47$	[21]
		$^1L_{Cu,Pb:Va}^{fcc} = 45684 + 5.151 \cdot T$	[24]
		$^0L_{Ag,Cu,Pb:Va}^{fcc} = -42022$	This work
	bcc: $(Ag, Cu, Pb, Va)_1 Va_3$	$^0L_{Ag,Cu:Va}^{bcc} = 12000$	[19]
		$^0L_{Ag,Pb:Va}^{bcc} = 20000$	[21]
		$^0L_{Cu,Pb:Va}^{bcc} = 20000$	[24]
	hcp: $(Ag, Cu, Pb)_1 Va_{0.5}$	$^0L_{Ag,Cu:Va}^{hcp} = 25000$	[19]
		$^0L_{Ag,Pb:Va}^{hcp} = 20000$	[21]
		$^0L_{Cu,Pb:Va}^{hcp} = 20000$	[24]

Temperature (T) in Kelvin and Gibbs energy in J/mol-formula. The Gibbs energies for the pure elements were taken from the SGTE database.[18] The thermodynamic parameters of the Ag–Cu,[19] Ag–Fe,[20] Ag–Pb,[21] Cu–Nb,[22] Cu–Fe[23] and Cu–Pb[24] binary systems were adopted in the present work.

and Cu–Pb[24] binary systems were directly adopted in the present work.

In the Ag–Cu–M (M = Nb, Fe, Pb) systems, no binary and ternary intermediate phases exist. The solution phases, i.e., liquid, fcc and bcc, were described by the substitutional solution model. The molar Gibbs energy of solution phase φ is expressed by the Redlich–Kister-Muggianu polynomial[25,26]

$$
\begin{aligned}
G^\varphi =\ & x_{Ag} \cdot {}^oG_{Ag}^\varphi + x_{Cu} \cdot {}^oG_{Cu}^\varphi + x_M \cdot {}^oG_M^\varphi \\
& + R \cdot T \cdot (x_{Ag} \cdot \ln x_{Ag} + x_{Cu} \cdot \ln x_{Cu} + x_M \cdot \ln x_M) \\
& + x_{Ag} \cdot x_{Cu} \cdot L_{Ag,Cu}^\varphi + x_{Ag} \cdot x_M \cdot L_{Ag,M}^\varphi + x_{Cu} \cdot x_M \cdot L_{Cu,M}^\varphi \\
& + x_{Ag} \cdot x_{Cu} \cdot x_M \cdot (x_{Ag} \cdot {}^0L_{Ag,Cu,M}^\varphi + x_{Cu} \cdot {}^1L_{Ag,Cu,M}^\varphi + x_M \cdot {}^2L_{Ag,Cu,M}^\varphi)
\end{aligned}
$$

(Eq 1)

where ${}^oG_i^\varphi$ stands for the Gibbs free energy of the pure component i (i = Ag, Cu or M) in the reference state for φ
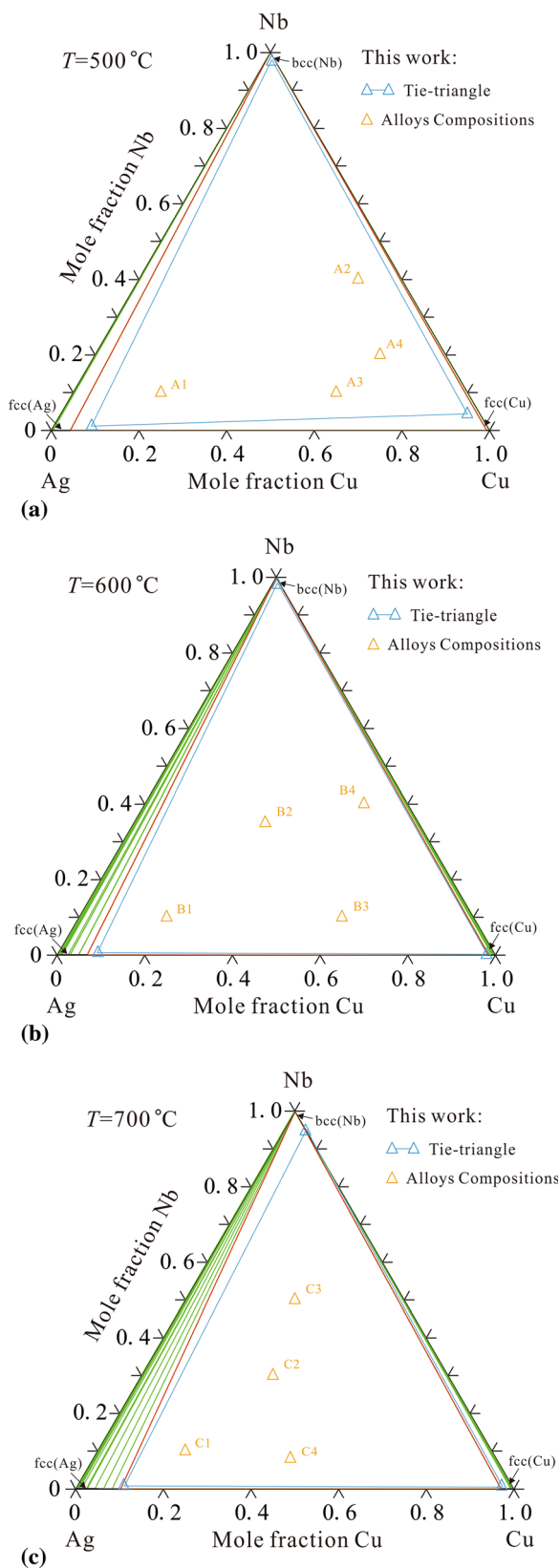
Fig. 4 Calculated isothermal sections of the Ag–Cu–Nb system along with the experimental data from the present work: (a) 500 °C; (b) 600 °C and (c) 700 °C

phase, R represents the gas constant, T is the temperature in Kelvin. x_{Ag}, x_{Cu} and x_M are the molar fractions of the elements Ag, Cu and M (M = Nb, Fe, Pb), respectively. The binary interaction parameters, $L_{Ag,Cu}^{\varphi}$, $L_{Ag,M}^{\varphi}$ and $L_{Cu,M}^{\varphi}$, as well as the ternary interaction parameters, ${}^{0}L_{Ag,Cu,M}^{\varphi}$, ${}^{1}L_{Ag,Cu,M}^{\varphi}$ and ${}^{2}L_{Ag,Cu,M}^{\varphi}$ are linearly temperature-dependent, which can be expressed as $L_{Ag,Cu,M}^{\varphi} = A + B \cdot T$. The coefficients A and B will be optimized according to the experimental data obtained from the present work and the literature.

4 Results and Discussion

4.1 Experimental Results and Discussion

Sixteen ternary alloys were prepared to determine the phase equilibria of the Ag–Cu–Nb system at 500, 600 and 700 °C. The experimental results of the phases identified by XRD, and the compositions and microstructures measured by SEM/EDS of the samples are summarized in Table 1.

The backscattered electron (BSE) micrographs and XRD patterns of the annealed alloys A2($Ag_{10}Cu_{50}Nb_{40}$) and A4($Ag_{15}Cu_{65}Nb_{20}$) at 500 °C, B3($Ag_{30}Cu_{60}Nb_{10}$) and B4($Ag_{10}Cu_{50}Nb_{40}$) at 600 °C and C1 ($Ag_{70}Cu_{20}Nb_{10}$) and C4 ($Ag_{47}Cu_{45}Nb_8$) at 700 °C are presented in Fig. 1 and 2. The microstructural analysis results of the equilibrated alloys A2, B3, B4, C1 and C4 presented in Fig. 1 clearly show three distinct phases, *i.e.*, the white, gray and dark phases, which correspond to fcc(Ag), bcc(Nb) and fcc(Cu), respectively. This is confirmed by XRD analysis shown in Fig. 2. The characteristic peaks of the three phases identified by XRD are distinctly described by the corresponding standard XRD spectral lines. Combined XRD patterns with EDS compositions analysis, A2, B3, B4, C1 and C4 are in fcc(Ag) + fcc(Cu) + bcc(Nb) three-phase region. The microstructure of alloy A4 presented in Fig. 2(b) shows the white and dark regions, which correspond to the fcc(Ag) and fcc(Cu) phases. According to the BSE micrograph and EDS compositions analysis, the existence of the bcc(Nb) phase could not be confirmed. The XRD diffraction patterns of the alloy A4 shown in Fig. 2(a) indicated that the alloy A4 contains the characteristic peaks of the bcc(Nb) phase as well as the ones of the fcc(Ag) and fcc(Cu) phases. Perhaps the bcc(Nb) phase is too fine to be measured by SEM, the BSE micrograph only shows two distinct contrasts. Thus, the alloy A4 is presumed to be in a three-phase region of fcc(Ag) + fcc(Cu) + bcc(Nb). Similarly, the phases and their compositions of the alloys A1 ($Ag_{70}Cu_{20}Nb_{10}$), A3 ($Ag_{30}Cu_{60}Nb_{10}$), B1($Ag_{70}Cu_{20}$-Nb_{10}), B2 ($Ag_{35}Cu_{30}Nb_{35}$), C2 ($Ag_{40}Cu_{30}Nb_{30}$) and C3

J. Phase Equilib. Diffus. (2022) 43:533–546

541

Fig. 5 Calculated liquidus projection of the Ag–Cu–Nb system
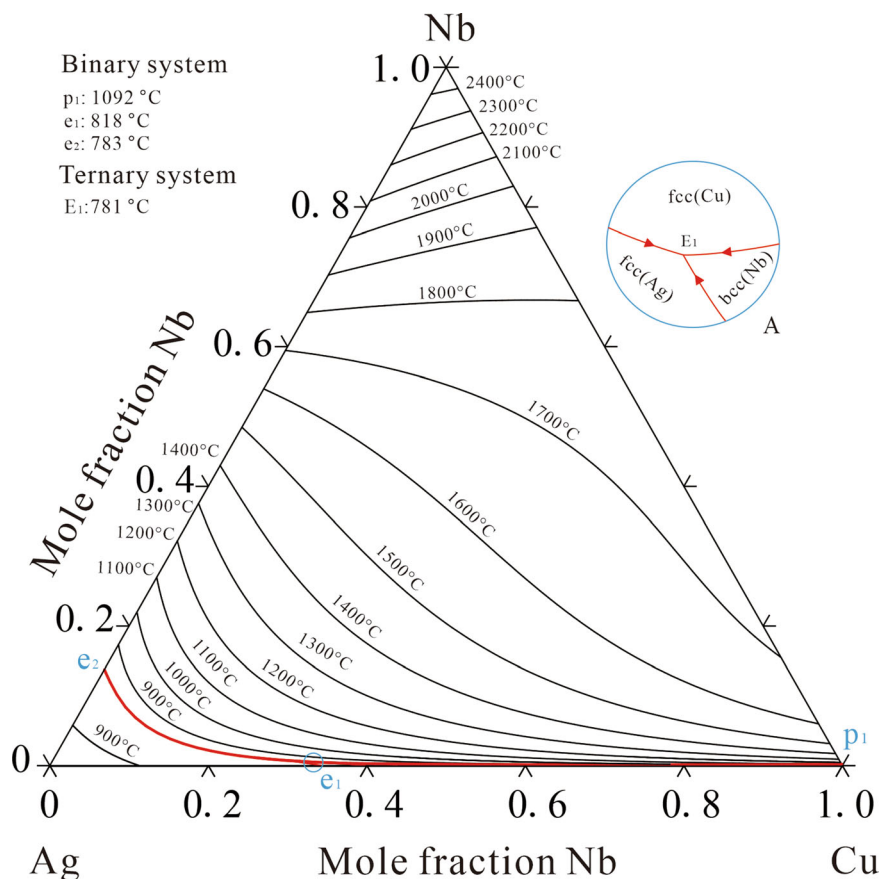
($Ag_{25}Cu_{25}Nb_{50}$) were analyzed and listed in Table 1. The alloys A1, A3, B1, B2, C2 and C3 are also located in the same three-phase region, fcc(Ag) + fcc(Cu) + bcc(Nb).

It is worth noting that the microstructures of the bcc(Nb) phase shown in Fig. 1(a), (c) and (d) are fine compared with the fcc(Ag) and fcc(Cu) phase regions. Though the center of the relatively larger phase region is selected when performing EDS measurements to avoid the influences of the surrounding phases or fine precipitates, the measured compositions of bcc(Nb) phase in alloys A1, B1, C2 and C3 are not reasonable and accurate and, therefore, are not used in the present work or listed in Table 1.

The measured average solubilities of Ag in the fcc(Cu) and bcc(Nb) phases, Cu in the fcc(Ag) and bcc(Nb) phases and Nb in the fcc(Ag) and fcc(Cu) phases are about 3.02, 0.57, 9.61, 2.96, 0.56 and 2.19 at.%, respectively. It can be noted that the solubilities of the third elements in the Ag–

Cu–Nb system at 500, 600 and 700 °C are less than 12 at.%.

Based on the experimental analysis above, the phase equilibria of Ag–Cu–Nb system at 500, 600 and 700 °C were obtained in the present work. For the isothermal sections at 500, 600 and 700 °C, the average compositions of the fcc(Ag), fcc(Cu) and bcc(Nb) phases among the experimental data of alloys A1–A4, B1–B4 and C1–C4 were selected to construct the experimental phase diagrams.

4.2 Thermodynamic Calculation Results and Discussion

In view of the little thermodynamic data, an optimization of the Ag–Nb system was carried out in the present work and the calculated phase diagram is presented in Fig. 3.
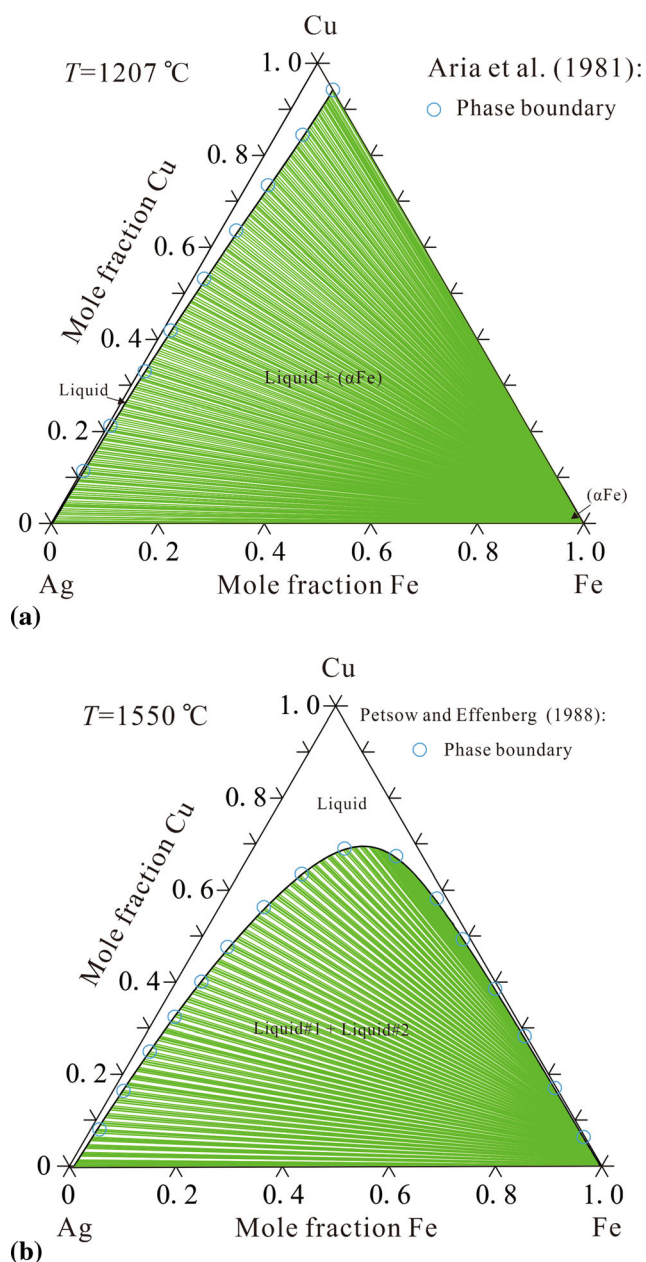
542

J. Phase Equilib. Diffus. (2022) 43:533–546

Fig. 6 Calculated isothermal sections of the Ag–Cu–Fe system along with the experimental data from literatures: (a) 1207 °C and (b) 1550 °C

Based on the available experimental data from the present work and literature,[19–24] the thermodynamic parameters of the Ag–Cu–M (M = Nb, Fe, Pb) systems are evaluated by the optimization module PARROT,[27,28] which works

by minimizing the square sum of the differences between the measured and the calculated values. The obtained thermodynamic parameters of the Ag–Cu–M (M = Nb, Fe, Pb) systems are listed in Table 2. Some representative phase diagrams of the Ag–Cu–M (M = Nb, Fe, Pb) systems are calculated. For consistency, mole fraction is adopted in the present work although weight fraction has been used in literature data.

4.2.1 The Ag–Cu–Nb System

The Ag–Cu–Nb system contains three solution phases, *i.e.*, fcc(Ag,Cu) and bcc(Nb), and the liquid phase appearing at 783 °C. Based on the experimental data, the Ag–Cu–Nb system was optimized, and the calculated isothermal sections at 500, 600 and 700 °C compared with the experimental phase equilibria data obtained in the present work are presented in Fig. 4(a) and (c), respectively. The comparison between the calculated isothermal sections and the experimental diagrams shows a good consistency. It is worthwhile mentioning that although the attempt was made to fit the parameters to the experimental data in optimization procedure, the calculated solubilities of Ag in the fcc(Cu) phase at 500 °C and Cu in bcc(Nb) at 700 °C are still larger than the experimental data.

As shown in Fig. 5, the liquidus projection of the Ag–Cu–Nb system with isotherms was calculated using the present thermodynamic parameters. An invariant reaction Liquid ↔ fcc(Ag) + fcc(Cu) + bcc(Nb) at 781 °C was predicted.

4.2.2 The Ag–Cu–Fe System

The calculated isothermal sections of the Ag–Cu–Fe system at 1207 and 1550 °C along with the experimental data reported by Aria et al.[19] and Petzow and Effenberg[20] were in good agreement with the measured ones. It also can be seen form Fig. 6(a) and (b) that the range of phase boundaries liquid/liquid + (αFe) and liquid/liquid#1 + liquid#2 were accurately calculated, and the liquid phase region increases with increasing temperature. The calculated solubility of Fe in the fcc (Cu) phase at 1207 °C is about 6.23 at.%, which shows a reasonable agreement with the measured one 5.98 at.%. As shown in Fig. 7, the liquidus projection of the Ag–Cu–Fe system with isotherms was calculated using the present thermodynamic parameters. The calculated liquidus temperatures reduces with the increase of Cu content, which is consistent with the experimental data reported by Lüder.[21] The

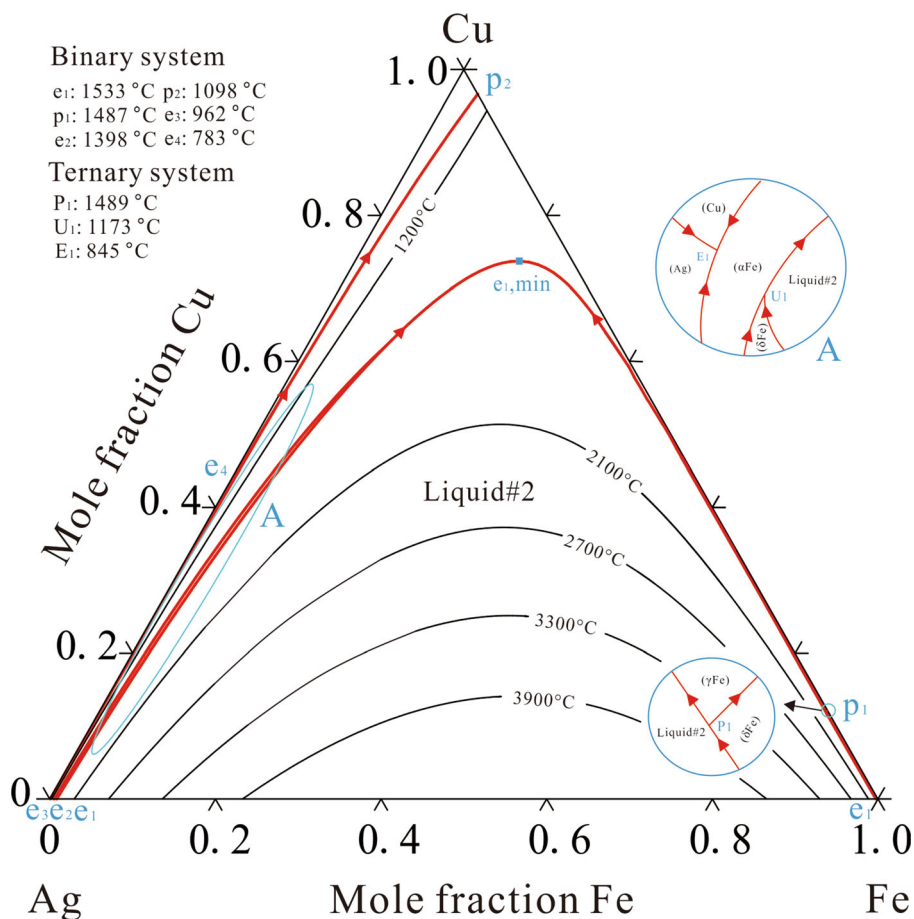**Fig. 7** Calculated liquidus projection of the Ag–Cu–Fe system

Table 3 Calculated invariant reactions in the Ag–Cu–Fe system

Type	Invariant reaction	Temperature, °C	Composition, at.%		
			Ag	Cu	Fe
P1	Liquid#1 + Liquid#2 + (δFe) ↔ (γFe)	1489	0.33	11.66	88.01
U1	Liquid#1 + (γFe) ↔ Liquid#2 + (αFe)	1173	82.44	16.68	0.88
E1	Liquid#1 ↔ (αFe) + (Ag) + (Cu)	845	43.46	56.03	0.51

predicted compositions and temperatures of the invariant reactions are listed in Table 3.

4.2.3 The Ag–Cu–Pb System

For the Ag–Cu–Pb system, the ternary interaction parameters of the liquid and fcc(Ag, Cu) were evaluated in the

present work to reproduce the experimental data reported by Petzow and Effenberg.[20] The calculated isothermal sections at 527 and 727 °C along with the experimental data[20] are presented in Fig. 8. The ranges of phase boundaries liquid/liquid + fcc(Ag) and liquid/liquid + fcc(Cu) were accurately calculated. It can be seen from Fig. 8 that one three-phase region,
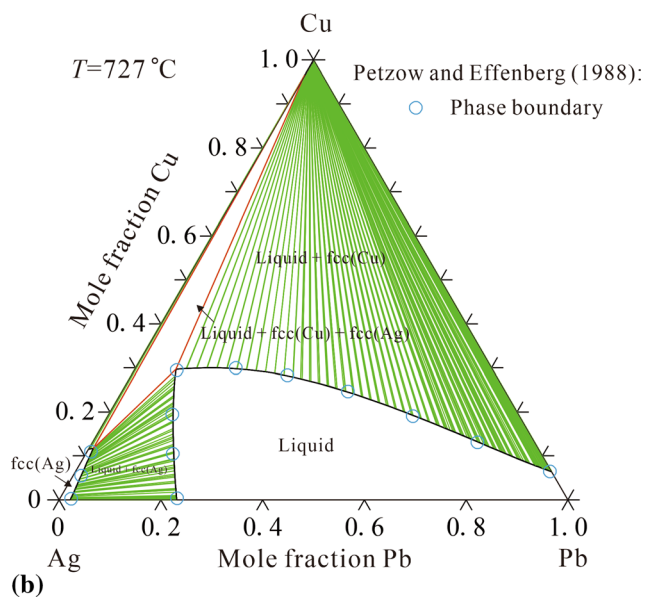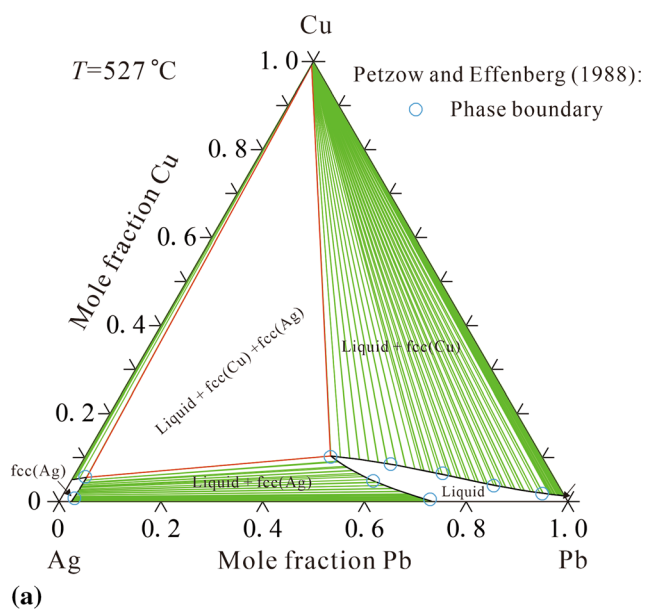
(a)

(b)

Fig. 8 Calculated isothermal sections of the Ag–Cu–Pb system along with the experimental data from literature: (a) 527 °C and (b) 727 °C

liquid + fcc(Ag) + fcc(Cu), at 527 and 727 °C was calculated and the liquid region enlarges with increasing temperature. Figure 9 shows the calculated liquidus projection of the Ag–Cu–Pb system over the entire composition range according to the present work. As shown in Fig. 9, the liquidus has two regions of primary solidification of fcc(Cu) and fcc(Ag). The calculated liquidus temperatures increase with the increasing of Cu content and a invariant reaction, Liquid ↔ fcc(Ag) + fcc(Cu) + fcc(Pb), occurs at 312 °C, which are consistent with the thermodynamic data reported by Petzow and Effenberg .[20]

In conjunction with the thermodynamic description for the Ag–Cu–M (M = Nb, Fe, Pb) systems a thermodynamic database for multi-component Ag–Cu alloys suitable for the extrapolation of the higher-order systems has been establishes and can provide important theoretical guidance in design and fabrication processing for new Ag–Cu alloys for solders or brazing materials.

5 Conclusions

- The phase equilibria of the Ag–Cu–Nb system at 500, 600 and 700 °C were experimentally investigated by means of the XRD and SEM/EDS methods. One three-phase region, *i.e.*, fcc(Ag) + fcc(Cu) + bcc(Nb), was determined. The solubilities of third elements in the binary system were measured and their values were generally less than 12 at.%.
- The thermodynamic assessment of the Ag–Cu–M (M = Nb, Fe, Pb) systems were carried out by using the CALPHAD method based on the experimental data available from the present work and literature. A set of the thermodynamic parameters of the Ag–Cu–M (M = Nb, Fe, Pb) systems was obtained. Some representative isothermal sections and liquidus projections were calculated. The present thermodynamic parameters can reproduce all the reliable experimental data.

Fig. 9 Calculated liquidus projection of the Ag–Cu–Pb system
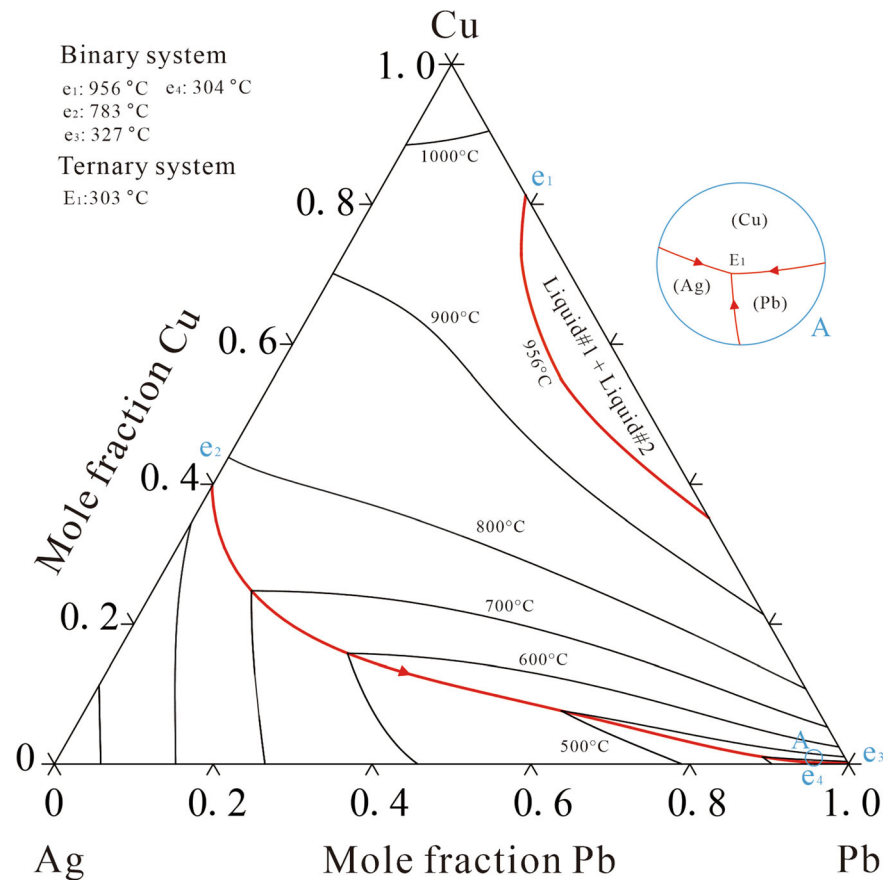
References

1. J.W. Choi, S. Kwon, Y. Park, K. Kang, and M.H. Lee, In Silico High-Throughput Screening of Ag-Based Electrocatalysts for Anion-Exchange Membrane Fuel Cells, *J. Phys. Chem. Lett.*, 2021, **12**, p 5660–5667.

2. T.A. Kassam, N.H. Babu, N. Ludford, S. Yan, and A. Howkins, Secondary Phase Interaction at Interfaces of High-Strength Brazed Joints Made Using Liquid Phase Sintered Alumina Ceramics and Ag–Cu–Ti Braze Alloys, *Sci. Rep.*, 2018, **8**, p 3352.

3. X.X. Wang, J. Peng, D.T. Cui, P. Xue, H. Li, A.M. Hu, and G.Y. Sun, Research and Application of Silver-Based Brazing Alloys in Manufacturing Industries: A Review, *Mater. Rep.*, 2018, **32**, p 1477–1485.

4. Y. Zhang, B. Hu, G. Zeng, S.H. Liu, Y. Du, and H.Q. Yin, Experimental Investigation Thermodynamic Modeling and Solidified Microstructure of the Cu–Ti–Nb termary System, *Calphad*, 2022, **76**, p 102395.

5. Y. Zhang, B. Hu, B.F. Li, M. Zhang, Q.P. Wang, and Y. Du, Experimental Investigation CALPHAD Modeling of the Cu–Cr–Si Ternary System, *Calphad*, 2021, **74**, p 102324.

6. Y. Zhang, B. Hu, Y.S. Shi, S.H. Liu, Y. Du, J.Q. Hu, Thermo-dynamic Modeling and Solidified Microstructure of the Ag–Sn–Zr Ternary System, T. Nonferr. Matel. Soc. (**in press**), 2022

7. R. Kieffer, S. Windisch, and H. Nowotny, Niobium-Tantalum, *Metall.*, 1963, **17**, p 669.

8. M.R. Baren, The Ag–Nb (silver-niobium) System, *Bull. Alloy Phase Diagr.*, 1989, **10**, p 640.

9. M. Aria, M. Tanaka, K.S. Goto, and M. Someno, Activity and Diffusivity Measurements of Copper in Gamma and Delta Fe by Equilibration between Solid Fe and liquid Ag, *Metall. Mater. Trans. A*, 1981, **12**, p 497–504.

10. G. Petzow, and G. Effenberg, Silver-Copper-Lead, *J. Mater. Res.*, 1988, **2**, p 1–13.

11. E. Lüder, Das Dreistoff-System, Silber-Kupfer-Eisen, *Z. Metallkd.*, 1924, **16**, p 61–62.

12. T. Klassen, U. Herr, and R.S. Averback, Mechanisms of Phase Formation during Milling in the Ternary Immiscible Ag–Cu–Fesystem, *Mat. Res. Soc. Symp. Proc.*, 1995, **400**, p 25–30.

13. H.Y. Gao, J. Wang, D. Shu, and B.D. Sun, Effect of Ag on the Microstructure and Properties of Cu–Fe in Situ Composites, *Scr. Mater.*, 2005, **53**, p 1105–1109.

14. Y.F. Wang, H.Y. Gao, J. Wang, Y.F. Han, Y.B. Dai, and B.D. Sun, First-Principles Calculation of Ag Addition on the Diffusion Mechanisms of Cu–Fe Alloys, *Solid State Commun.*, 2014, **183**, p 60–63.

15. W.L. Jiang, C. Zhang, N. Xu, B. Yang, B.Q. Xu, D.C. Liu, and H.W. Yang, Experimental Investigation and Modelling of Phase

546

J. Phase Equilib. Diffus. (2022) 43:533–546

Equilibria for the Ag–Cu–Pb System in Vacuum Distillation, *Fluid Phase Equilib.*, 2016, **417**, p 19–24.

16. Z.K. Liu, and Y. Wang, *Computational thermodynamics of materials*. Cambridge University Press, New York, 2016.

17. H. Lukas, S.G. Fries, and B. Sundman, *Computational thermodynamics: the Calphad method*. Cambridge University Press, New York, 2007.

18. A.T. Dinsdale, SGTE Data for Pure Elements, *Calphad*, 1991, **15**, p 317–425.

19. X.C. He, H. Wang, H.S. Liu, and Z.P. Jin, Thermodynamic Description of the Cu–Ag–Zr System, *Calphad*, 2006, **30**, p 367–374.

20. J.Q. Zhou, B. Hu, Y. Jiang, C.L. Qiu, Y. Du, and H.Q. Yin, Thermodynamic Modeling of the Ag–X (X=B, Fe, Sm, Pu) Binary System, *J. Phase Equilib. Diffus.*, 2020, **41**, p 257–268.

21. B.Z. Lee, C.S. Oh, and D.N. Lee, A thermodynamic Evaluation of the Ag–Pb–Sb System, *J. Alloys Compd.*, 1994, **215**, p 293–301.

22. G.I. Terekhov, and L.N. Aleksandrova, The Copper–Niobium Phase Diagram, *Izv. Akad. Nauk. SSSR. Met.*, 1984, **4**, p 210–213.

23. I. Ansara, and A. Jansson, System Cu-Fe, in *COST 507*, Vol. 2. I. Ansara, A.T. Dinsdale, and M.H. Rand, Eds., European Communities, Brussels, 1998, p 165–167

24. B. Onderka, and L. Zabdyr, A New Critical Assessment of the Copper-Lead System, *Scand. J. Metall.*, 2001, **30**, p 320–323.

25. O. Redlich, and A.T. Kister, Thermodynamics of Nonelectrolyte Solutions x–y–t Relations in a Binary System, *Ind. Chem. Phys.*, 1948, **40**, p 341–345.

26. Y.M. Muggianu, M. Gambino, and J.P. Bros, Enthalpies of Formation of Liquid Alloys Bismuth-Gallium-Tin at 723k - Choice of an Analytical Representation of Integral and Partial Thermodynamic Functions of Mixing for this Ternary-System, *J. Chim. Phys. Phys. -Chim. Biol.*, 1975, **72**, p 83–88.

27. B. Sundman, and J. Agren, A Regular Solution Model for Phases with Several Components and Sublattices Suitable for Computer Applications, *J. Phys. Chem. Solids*, 1981, **42**, p 297–301.

28. B. Sundman, B. Jansson, and J.O. Andersson, The Thermo-Calc Databank System, *Calphad*, 1985, **9**, p 153–190.